

FROM SPECIALIST TO GENERALIST: UNLOCKING SAM’S LEARNING POTENTIAL ON UNLABELED MEDICAL IMAGES

Vi Vu^{1*}, Thanh-Huy Nguyen^{1*}, Tien-Thinh Nguyen^{2*}, Ba-Thinh Lam³
 Hoang-Thien Nguyen¹, Tianyang Wang⁴, Xingjian Li¹, Min Xu^{1†}

¹ Carnegie Mellon University, USA

² Industrial University of Ho Chi Minh City, Vietnam

³ University of North Carolina at Charlotte, USA

⁴ University of Alabama at Birmingham, USA

ABSTRACT

Foundation models like the Segment Anything Model (SAM) show strong generalization, yet adapting them to medical images remains difficult due to domain shift, scarce labels, and the inability of Parameter-Efficient Fine-Tuning (PEFT) to exploit unlabeled data. While conventional models like U-Net excel in semi-supervised medical learning, their potential to assist a PEFT SAM has been largely overlooked. We introduce **SC-SAM**, a specialist-generalist framework where U-Net provides point-based prompts and pseudo-labels to guide SAM’s adaptation, while SAM serves as a powerful generalist supervisor to regularize U-Net. This reciprocal guidance forms a bidirectional co-training loop that allows both models to effectively exploit the unlabeled data. Across prostate MRI and polyp segmentation benchmarks, our method achieves state-of-the-art results, outperforming other existing semi-supervised SAM variants and even medical foundation models like MedSAM, highlighting the value of specialist–generalist cooperation for label-efficient medical image segmentation. Our code is available at <https://github.com/vnlvi2k3/SC-SAM>.

Index Terms— Foundation Model, Domain Shift, Semi-supervised Learning, Medical Image Segmentation

1. INTRODUCTION

Foundation models have reshaped image segmentation through large-scale pre-training, with the *Segment Anything Model* (SAM) [1] showing impressive prompt-driven zero-shot performance. However, SAM struggles in medical imaging due to the significant domain gap, scarce annotations, and the instability of tuning a large model with limited labels. Parameter-Efficient Fine-Tuning (PEFT) reduces computation but still relies heavily on labeled data, leaving the abundant unlabeled medical images underutilized.

Meanwhile, conventional architectures such as U-Net have shown, over years of semi-supervised research, that unlabeled data can be a powerful asset. Techniques like consistency regularization and pseudo-labeling allow these models to extract reliable structures from unannotated images. Interestingly, although U-Nets excel at learning from unlabeled data, SAM does not naturally inherit this ability. SemiSAM+ [2] prompts a frozen SAM using a specialist. KnowSAM [3] distills SAM into lighter networks. CPC-SAM [4] enforces cross-prompt consistency between dual SAM decoders. These methods demonstrate various uses of SAM but also introduce architectural complexity or rely solely on SAM’s predictions. It leaves open the question of whether a conventional model could meaningfully help a PEFT SAM learn from unlabeled data.

This observation motivates our approach. We propose *SC-SAM: Specialist Co-training with SAM*, a specialist-generalist collaboration framework that leverages the complementary strengths of U-Net and SAM. Instead of treating SAM as a primary supervisor, we invert the direction: U-Net first learns from both labeled and unlabeled data using standard semi-supervised strategies, and its predictions are then transformed into point-based prompts and pseudo-labels that guide SAM during PEFT. In parallel, SAM generates refined masks that regularize and stabilize U-Net’s training. This forms a *bidirectional co-training loop* in which U-Net contributes structural domain knowledge, and SAM serves as a high-level semantic regularizer. The two models progressively align, allowing SAM to benefit directly from unlabeled information.

Across various medical image segmentation benchmarks, *SC-SAM* achieves consistent improvements over existing semi-supervised SAM variants and even surpasses strong medical foundation models such as MedSAM and SAM-Med-2D. Our results point to a simple but underexplored principle: Cooperation between conventional specialists and modern generalist models can unlock new pathways for scalable, label-efficient medical image segmentation.

† Corresponding Author

* Equal contribution.

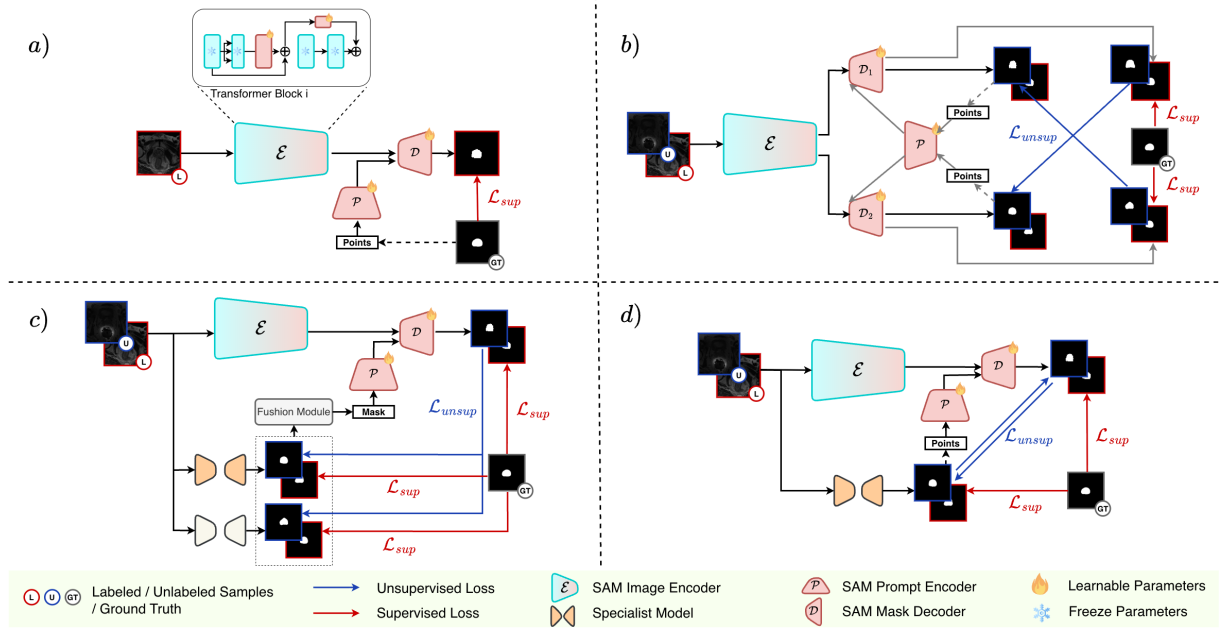


Fig. 1. Overview of different techniques for incorporating SAM in semi-supervised settings: a) PEFT-SAM, b) Dual-SAM, c) SP-SAM, and d) SC-SAM (Ours)

2. METHODOLOGY

In semi-supervised segmentation, the training set consists of a labeled set $D_l = \{(X_i^l, Y_i^l)\}_{i=1}^N$, and a larger unlabeled set $D_u = \{(X_j^u)\}_{j=1}^M$ ($M \gg N$). Each image $X \in \mathbb{R}^{C \times H \times W}$ has $C = 3$ for RGB or $C = 1$ for grayscale inputs, and each labeled sample X_i^l is paired with a ground-truth mask Y_i^l . We next outline existing techniques for incorporating SAM in semi-supervised settings: PEFT-SAM, Dual-SAM, and SP-SAM, and show how their limitations give rise to our method, SC-SAM.

PEFT-SAM: Parameter-efficient Fine-tuning of SAM on labeled set. To adapt SAM on the limited labeled data, we apply PEFT by introducing learnable Adapter layers [5] into each Transformer block of its image encoder \mathcal{E} , while prompt encoder \mathcal{P} and mask decoder \mathcal{D} are kept trainable with negligible additional parameters as outlined in Fig. 1(a). Point prompts are sampled from the ground-truth masks of the labeled set and, together with the encoder's image embeddings, are fed into the decoder to obtain the predictions:

$$\text{points} = \text{Sample}(Y^l)$$

$$P_{SAM}^l = \mathcal{D}(\mathcal{E}(X^l), \mathcal{P}(\text{points})),$$

where $\text{Sample}(\cdot)$ randomly selects five foreground and five background points from the ground truth. The supervised loss \mathcal{L}_{seg} is the mean of Dice and Cross-Entropy losses:

$$\mathcal{L}_{sup} = \mathcal{L}_{seg}(\text{softmax}(P_{SAM}^l), Y^l)$$

Dual-SAM: Leveraging unlabeled data with Dual-branch SAM

Miao *et al.* [4] introduced a dual-decoder SAM framework, where each decoder generates prompts and provides cross-supervision to the other. We denote \mathcal{D}_1 and \mathcal{D}_2 as two distinct learnable decoders (see Fig. 1 (b)).

Phase 1:

$$P_{1,2}^{l,u} = \mathcal{D}_{1,2}(\mathcal{E}(X^{u,l}))$$

$$\text{points}_{1,2} = \text{Sample}(P_{1,2}^{l,u})$$

Phase 2:

$$P_1^{l,u} = \mathcal{D}_1(\mathcal{E}(X^{u,l}), \text{points}_2), \quad P_2^{l,u} = \mathcal{D}_2(\mathcal{E}(X^{u,l}), \text{points}_1)$$

The pseudo-label $\hat{P} = \arg \max(P)$ is obtained from the model prediction for computing the unsupervised loss:

$$\mathcal{L}_{sup} = \mathcal{L}_{seg}(P_1^l, Y^l) + \mathcal{L}_{seg}(P_2^l, Y^l)$$

$$\mathcal{L}_{unsup} = \mathcal{L}_{seg}(P_1^u, \hat{P}_2^u) + \mathcal{L}_{seg}(P_2^u, \hat{P}_1^u)$$

SP-SAM: Specialist-guided Prompting for SAM fine-tuning

Fig. 1 (c) represents the work of Huang *et al.* [3], which integrates two specialists (or conventional networks) UNet [6] \mathcal{S}_1 and VNet [7] \mathcal{S}_2 , together with a learnable fusion module \mathcal{F} that fuses their predicted masks to generate mask prompts for SAM:

$$P_{1,2}^{l,u} = S_{1,2}(X^{l,u})$$

$$\text{mask} = \mathcal{F}(P_1^{l,u}, P_2^{l,u})$$

$$P_{SAM}^{l,u} = \mathcal{D}(\mathcal{E}(X^{l,u}), \mathcal{P}(\text{mask}))$$

Through knowledge distillation, SAM supervises the specialists and allows them to exploit the unlabeled set to produce more robust prompts for SAM fine-tuning.

$$\mathcal{L}_{\text{sup}} = \mathcal{L}_{\text{seg}}(P_1^l, Y^l) + \mathcal{L}_{\text{seg}}(P_2^l, Y^l) + \mathcal{L}_{\text{seg}}(P_{\text{SAM}}^l, Y^l)$$

$$\mathcal{L}_{\text{unsup}} = \mathcal{L}_{\text{KD}}(P_1^u, \hat{P}_{\text{SAM}}^u) + \mathcal{L}_{\text{KD}}(P_2^u, \hat{P}_{\text{SAM}}^u),$$

where L_{KD} is the Kullback–Leibler divergence loss.

SC-SAM: Specialist Co-training with SAM. *PEFT-SAM* focuses on fine-tuning SAM using limited labeled data or adopt zero or few-shot tuning, leaving the unlabeled set under-exploited. *Dual-SAM* leverages unlabeled data through dual-branch cross-supervision; however, under significant domain shift in semi-supervised medical image segmentation, generalist models like SAM are prone to overconfident predictions, leading both branches to step into coupling problem and converge to similar local minima. In contrast, specialist networks (e.g., UNet) trained from scratch can correct SAM’s high-confidence false predictions. Unlike *SP-SAM*, which exclusively exploits specialist strengths only for robust prompting, our goal is to collaboratively train generalist and specialist networks to form a bi-directional co-training loop (see Fig. 1 (d)).

$$P_{\text{UNet}}^{l,u} = \mathcal{S}(X^{l,u}) \quad (1)$$

$$\text{points} = \text{Sample}(P_{\text{UNet}}^{l,u}) \quad (2)$$

$$P_{\text{SAM}}^{l,u} = \mathcal{D}(\mathcal{E}(X^l), \mathcal{P}(\text{points})) \quad (3)$$

However, naive co-training is unstable due to the disparity in convergence behaviors: SAM shows superior early-stage performance to serve as an effective regularizer for UNet but also suffer from early overfitting, while UNet converges slowly yet ultimately adapts better to the target domain. Directly transferring supervision signals from UNet to SAM causes noisy unlabeled signals dominate in the early unsupervised phase and corrupt SAM. We thereby design a sigmoid ramp-up strategy as follows:

$$\mathcal{L}_{\text{sup}} = \mathcal{L}_{\text{seg}}(P_{\text{UNet}}^l, Y^l) + \mathcal{L}_{\text{seg}}(P_{\text{SAM}}^l, Y^l) \quad (4)$$

$$\mathcal{L}_{\text{unsup}} = \mathcal{L}_{\text{seg}}(P_{\text{UNet}}^u, \hat{P}_{\text{SAM}}^u) + \omega(t) \mathcal{L}_{\text{seg}}(P_{\text{SAM}}^u, \hat{P}_{\text{UNet}}^u) \quad (5)$$

$$\omega(t) = \begin{cases} e^{-(1 - \frac{t}{T_{\text{max}}})^2}, & 0 \leq t \leq T_{\text{max}}, \\ 1, & t > T_{\text{max}} \end{cases} \quad (6)$$

where t and T_{max} are the current iteration and the ramp up length, respectively. The final training objective is:

$$\mathcal{L}_{\text{total}} = \mathcal{L}_{\text{sup}} + \mathcal{L}_{\text{unsup}} \quad (7)$$

3. EXPERIMENT RESULTS

All experiments were performed on a single NVIDIA RTX 3090 Ti GPU (24 GB RAM) using Python 3.10, PyTorch 2.9, and CUDA 12.8. We used Adam optimizer (initial learning

rate 10^{-4}) for SAM and SGD (momentum 0.9) for UNet. The batch size was set to 24, consisting of 12 labeled and 12 unlabeled samples. For labeled samples, we applied a weak augmentation pipeline including random flipping, brightness and contrast adjustments, shift-scale-rotate, and dropout. For unlabeled samples, we additionally used stronger augmentations such as grid distortion and shift-scale-rotate. For *PEFT-SAM* and *SC-SAM*, we also employed learnable bounding box prompts following *SP-SAM* [3].

3.1. Datasets

We evaluated our method on two public medical image segmentation benchmarks. The **PROMISE12** [8] dataset consists of 50 prostate MR volumes, split into 35/5/10 for train/val/test. Slices within each MRI volume were treated as 2D images. For the **COLON** dataset, we used 612 endoscopic images from CVC-ClinicDB [9] and 838 images from Kvasir [10], and evaluated the cross-dataset generalization on five benchmark test sets: CVC-300 [11], CVC-ColonDB [12], CVC-ClinicDB, ETIS-LaribPolypDB [13], and Kvasir-SEG [10]. For both datasets, only 5% or 10% of the training images were provided with annotations.

3.2. Quantitative results

Table 1. Quantitative results on the **PROMISE12** dataset.

Spec.	Labeled ratio	5%				10%			
		Dice	IoU	HD95	ASD	Dice	IoU	HD95	ASD
✗	SAM [1]	72.26	59.39	4.25	8.79	79.66	68.53	4.02	5.79
	MedSAM [14]	63.00	48.65	4.85	14.91	74.75	62.12	4.28	7.45
	SAM-Med2D [15]	49.18	35.85	10.74	15.58	62.78	48.49	4.51	9.29
	CPC-SAM [4]	73.73	62.48	26.49	10.22	80.42	70.75	12.04	5.99
✓	KnowSAM [3]	78.49	67.16	4.11	6.40	82.93	73.18	3.94	3.92
✓	Ours	83.64	73.87	3.98	3.79	83.35	73.54	3.91	3.81

We report Dice coefficient, Intersection-over-Union (IoU), Average Surface Distance (ASD), and the 95th percentile Hausdorff Distance (HD95) for quantitative evaluation. Our proposed *SC-SAM* was compared with several state-of-the-art baselines: For *PEFT-SAM*, we adopted SAM [1], SAM-Med2D [15], MedSAM [14] as backbones; we used KnowSAM [3] to represent *SP-SAM*, and CPC-SAM [4] for *Dual-SAM*. As shown in Tab. 1 and 2, our method consistently achieves superior performance when trained with 5% and 10% labeled settings on PROMISE12 and COLON datasets. Especially at the 5% labeled ratio, our *SC-SAM* outperforms KnowSAM by a large margin, which ranks second in nearly all settings, highlighting that, in addition to using the specialists for prompt creation, effectively leveraging them to generate pseudo-labels for potential unlabeled data is critical. For *PEFT-SAM* methods, SAM achieves higher accuracy than the medical SAM models, highlighting its strong generalizability when fine-tuned on limited data of the target domain. CPC-SAM performs relatively poorly, suggesting that leveraging UNet as a supervisor for unlabeled

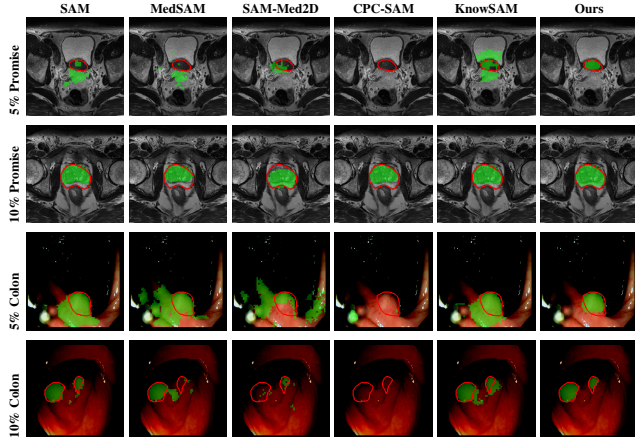
Table 2. Quantitative results of different methods on the Colon datasets on 5% and 10% labeled fractions.

Labeled ratio	Spec. Avail	Dataset	CVC-300		CVC-ClinicDB		CVC-ColonDB		ETIS-Larib		Kvasir	
			Model	Dice (\uparrow)	IoU (\uparrow)	Dice (\uparrow)	IoU (\uparrow)	Dice (\uparrow)	IoU (\uparrow)	Dice (\uparrow)	IoU (\uparrow)	
5%	\times	SAM [1]	82.02	73.13	74.27	65.93	60.82	52.37	51.09	42.68	82.79	75.09
		MedSAM [14]	17.56	12.36	49.97	41.39	16.85	11.57	12.38	15.65	54.88	42.68
		SAM-Med2D [15]	14.09	8.10	41.73	31.22	18.73	11.45	13.09	7.70	38.73	26.23
		CPC-SAM [4]	55.56	50.52	61.05	54.73	44.68	40.17	37.62	34.11	80.87	74.26
10%	\checkmark	KnowSAM [3]	83.75	75.2	78.86	70.93	66.76	58.14	56.72	47.36	84.78	77.03
		Ours	88.72	80.56	79.54	73.21	67.77	58.97	56.91	49.85	84.79	77.45
		SAM [1]	83.33	74.89	79.64	72.46	66.74	58.17	57.46	49.5	85.54	78.25
		MedSAM [14]	27.42	20.82	59.33	49.79	22.18	15.89	23.45	17.18	57.42	45.29
10%	\checkmark	SAM-Med2D [15]	13.59	7.78	49.29	36.9	17.63	10.8	15.44	9.39	41.66	28.51
		CPC-SAM [4]	75.66	69.05	57.8	51.92	47.53	43.01	33.53	31.67	79.78	73.59
		KnowSAM [3]	86.49	78.65	82.54	75.26	68.21	60.04	64.11	55.46	86.64	79.58
		Ours	88.17	80.79	83.06	77.05	68.69	60.60	60.07	52.97	86.27	79.52

data eliminates its over-confidence and coupling issues more effectively than using another SAM.

3.3. Qualitative results

Table 3. Qualitative results of different methods,  and  denote groundtruth and predicted mask, respectively.



For the qualitative results shown in Tab. 3, our method consistently produces more accurate and compact segmentation results for most cases in the PROMISE12 and COLON datasets, effectively capturing the prostate and polyp boundaries while suppressing background noise. In contrast, other approaches tend to over-segment the target regions, leading to the inclusion of irrelevant surrounding tissues. These results visually demonstrate the robustness of our method in handling diverse anatomical variations.

3.4. Ablation Study

To ascertain the effectiveness of each component in our framework, we performed ablation studies on both the specialist backbone selection and the use of a sigmoid ramp-up

during unsupervised phase. As shown in Tab. 4, directly transferring supervision from UNet to SAM without ramp-up caused noisy unlabeled signals to dominate the early stage of SAM tuning, resulting in a 47% drop in Dice score. Replacing the UNet specialist with UNet++ [16] or ResUNet++ [17] yielded lower performance. Swin-UNet [18] performs as a less effective pseudo-label generator than CNN-based backbones due to the data-hungry nature of ViTs in semi-supervised settings.

Table 4. Ablation study on sigmoid ramp-up and specialist backbones with 5% labeled data on PROMISE12 dataset.

Backbone	Ramp-up	Dice	IoU	HD95	ASD
UNet [6]		36.37	29.46	47.26	49.07
SwinUNet [18]	\checkmark	70.27	56.44	4.26	8.12
ResUNet++ [17]	\checkmark	78.20	66.32	4.09	5.17
UNet++ [16]	\checkmark	80.14	68.87	4.05	4.56
UNet [6]	\checkmark	83.64	73.87	3.98	3.79

4. CONCLUSION

We presented *SC-SAM*, a specialist-generalist framework that enables U-Net to guide a PEFT SAM in leveraging unlabeled medical images. Through a stable bidirectional co-training loop, U-Net provides structural cues while SAM offers refined semantic regularization, allowing SAM to benefit directly from semi-supervised learning. Experiments on prostate MRI and polyp segmentation show that *SC-SAM* surpasses recent semi-supervised SAM variants and even strong medical foundation models. These results demonstrate that combining a conventional specialist with a powerful generalist offers an effective and label-efficient strategy for medical image segmentation.

5. ACKNOWLEDGMENT

This work was supported in part by U.S. NIH grant R35GM158094. We thank AI VIETNAM for supporting us with GPUs to conduct experiments.

6. REFERENCES

[1] Alexander Kirillov, Eric Mintun, Nikhila Ravi, Hanzi Mao, Chloe Rolland, Laura Gustafson, Tete Xiao, Spencer Whitehead, Alexander C Berg, Wan-Yen Lo, et al., “Segment anything,” in *Proceedings of the IEEE/CVF international conference on computer vision*, 2023, pp. 4015–4026.

[2] Yichi Zhang, Bohao Lv, Le Xue, Wenbo Zhang, Yuchen Liu, Yu Fu, Yuan Cheng, and Yuan Qi, “Semisam+: Rethinking semi-supervised medical image segmentation in the era of foundation models,” *arXiv preprint arXiv:2502.20749*, 2025.

[3] Kaiwen Huang, Tao Zhou, Huazhu Fu, Yizhe Zhang, Yi Zhou, Chen Gong, and Dong Liang, “Learnable prompting sam-induced knowledge distillation for semi-supervised medical image segmentation,” *IEEE Transactions on Medical Imaging*, 2025.

[4] Juzheng Miao, Cheng Chen, Keli Zhang, Jie Chuai, Quanzheng Li, and Pheng-Ann Heng, “Cross prompting consistency with segment anything model for semi-supervised medical image segmentation,” in *International Conference on Medical Image Computing and Computer-Assisted Intervention*. Springer, 2024, pp. 167–177.

[5] Junde Wu, Ziyue Wang, Mingxuan Hong, Wei Ji, Huazhu Fu, Yanwu Xu, Min Xu, and Yueming Jin, “Medical sam adapter: Adapting segment anything model for medical image segmentation,” *Medical image analysis*, vol. 102, pp. 103547, 2025.

[6] Olaf Ronneberger, Philipp Fischer, and Thomas Brox, “U-net: Convolutional networks for biomedical image segmentation,” in *International Conference on Medical image computing and computer-assisted intervention*. Springer, 2015, pp. 234–241.

[7] Fausto Milletari, Nassir Navab, and Seyed-Ahmad Ahmadi, “V-net: Fully convolutional neural networks for volumetric medical image segmentation,” in *2016 fourth international conference on 3D vision (3DV)*. Ieee, 2016, pp. 565–571.

[8] Geert Litjens, Robert Toth, Wendy Van De Ven, Caroline Hoeks, Sjoerd Kerkstra, Bram Van Ginneken, Graham Vincent, Gwenael Guillard, Neil Birbeck, Jindang Zhang, et al., “Evaluation of prostate segmentation algorithms for mri: the promise12 challenge,” *Medical image analysis*, vol. 18, no. 2, pp. 359–373, 2014.

[9] Jorge Bernal, F Javier Sánchez, Gloria Fernández-Esparrach, Debora Gil, Cristina Rodríguez, and Fernando Vilariño, “Wm-dova maps for accurate polyp highlighting in colonoscopy: Validation vs. saliency maps from physicians,” *Computerized medical imaging and graphics*, vol. 43, pp. 99–111, 2015.

[10] Debesh Jha, Pia H Smedsrød, Michael A Riegler, Pål Halvorsen, Thomas De Lange, Dag Johansen, and Håvard D Johansen, “Kvasir-seg: A segmented polyp dataset,” in *International conference on multimedia modeling*. Springer, 2019, pp. 451–462.

[11] David Vázquez, Jorge Bernal, F Javier Sánchez, Gloria Fernández-Esparrach, Antonio M López, Adriana Romero, Michal Drozdzał, and Aaron Courville, “A benchmark for endoluminal scene segmentation of colonoscopy images,” *Journal of healthcare engineering*, vol. 2017, no. 1, pp. 4037190, 2017.

[12] Nima Tajbakhsh, Suryakanth R Gurudu, and Jianming Liang, “Automated polyp detection in colonoscopy videos using shape and context information,” *IEEE transactions on medical imaging*, vol. 35, no. 2, pp. 630–644, 2015.

[13] Juan Silva, Aymeric Histace, Olivier Romain, Xavier Dray, and Bertrand Granado, “Toward embedded detection of polyps in wce images for early diagnosis of colorectal cancer,” *International journal of computer assisted radiology and surgery*, vol. 9, no. 2, pp. 283–293, 2014.

[14] Jun Ma, Yuting He, Feifei Li, Lin Han, Chenyu You, and Bo Wang, “Segment anything in medical images,” *Nature Communications*, vol. 15, no. 1, pp. 654, 2024.

[15] Junlong Cheng, Jin Ye, Zhongying Deng, Jianpin Chen, Tianbin Li, Haoyu Wang, Yanzhou Su, Ziyan Huang, Jilong Chen, Lei Jiang and Hui Sun, Junjun He, Shaoting Zhang, Min Zhu, and Yu Qiao, “Sam-med2d,” 2023.

[16] Zongwei Zhou, Md Mahfuzur Rahman Siddiquee, Nima Tajbakhsh, and Jianming Liang, “Unet++: A nested u-net architecture for medical image segmentation,” in *International workshop on deep learning in medical image analysis*. Springer, 2018, pp. 3–11.

[17] Debesh Jha, Pia H Smedsrød, Michael A Riegler, Dag Johansen, Thomas De Lange, Pål Halvorsen, and Håvard D Johansen, “Resunet++: An advanced architecture for medical image segmentation,” in *2019 IEEE international symposium on multimedia (ISM)*. IEEE, 2019, pp. 225–2255.

[18] Hu Cao, Yueyue Wang, Joy Chen, Dongsheng Jiang, Xiaopeng Zhang, Qi Tian, and Manning Wang, “Swin-unet: Unet-like pure transformer for medical image segmentation,” in *European conference on computer vision*. Springer, 2022, pp. 205–218.